Applied Thermal Engineering 73 (2014) 152–159

Contents lists available at ScienceDirect

Applied Thermal Engineering

journal homepage: www.elsevier.com/locate/apthermeng

Feasibility study of Boron Nitride coating on Lithium-ion battery casing

L.H. Saw*, Y. Ye [1], A.A.O. Tay [1]

Department of Mechanical Engineering, Faculty of Engineering, National University of Singapore, 117576 Singapore, Singapore

HIGHLIGHTS

- We studied the Boron Nitride coating on battery casing using Taguchi method.
- We investigated the effect of surface roughness and coating thickness on adhesion strength.
- We compared the effect of coating and polymer insulator in heat transfer.
- The Boron Nitride coating could enhance the thermal management of the battery.

ARTICLE INFO

Article history:
Received 21 March 2014
Accepted 28 June 2014
Available online 18 July 2014

Keywords:
Taguchi method
Battery temperature
Coating
Optimization
Heat transfer

ABSTRACT

Increasing in public awareness about global warming and exhaustion of energy resources has led to a flourishing electric vehicle industry that would help realize a zero-emission society. The thermal management of battery packs, which is an essential issue closely linked to a number of challenges for electric vehicles including cost, safety, reliability and lifetime, has been extensively studied. However, relatively little is known about the thermal effect of polymer insulation on the Lithium-ion battery casing. This study investigates the feasibility of replacing the polymer insulation with a Boron Nitride coating on the battery casing using the Taguchi experimental method. The effect of casing surface roughness, coating thickness and their interaction were examined using orthogonal array L_9 (3^4). Nominal the best is chosen for the optimization process to achieve optimum adhesion strength. In addition, the thermal improvements of the coating as compared to conventional polymer insulator on the battery are further investigated.

1. Introduction

Lithium-ion battery with its high energy and power per unit mass, no memory effect and relatively long cycle life as compared to Nickel Metal Hydride and lead acid battery has received vast attention recently especially in portable electronic devices and automotive applications. The battery cells are connected in series and in parallel and close packed to provide the necessary power for the devices [1]. Although Lithium-ion battery possesses an immense potential in automotive and aerospace application, its thermal and safety problems remain critical issue yet to be resolved, especially in the development of fast charging battery [2,3]. Thermal management is an important issue in Lithium-ion batteries, because the electrochemical process in the battery is vulnerable to the temperature variation. At high I_t-rate of charging or discharging, the exothermic heat generated in the cell and inadequate cooling eventually lead to thermal aging and thermal runaway [2]. Besides, uneven temperature distribution in the cell or module reduces the cycle life and charging capacity [3].

Insulation of the battery body is extremely important for a battery so that the positive and negative terminals are isolated. Good insulation is desirable to prevent any short circuit and sparks that occur when the cells are closely packed. In general, insulation material for the battery body is made of polymer such as Polyvinyl Chloride (PVC) or Polyethylene Terephthalate (PET) and a heat shrink is wrapped around the battery body as shown in Fig. 1. The thickness of the insulating film is about 0.2–0.3 mm. The polymer insulator must endure a harsh environment that composes of thermal cycling during charging and discharging cycle and corrosive environment which could cause insulator degradation, fracture

* Corresponding author. Tel.: +65 65162207; fax: +65 67791459.
E-mail addresses: bernardsaw81@yahoo.com, bernardsaw@nus.edu.sg (L.H. Saw), mpetayao@nus.edu.sg (A.A.O. Tay).
[1] Tel.: +65 65162207; fax: +65 67791459.

http://dx.doi.org/10.1016/j.applthermaleng.2014.06.061
1359-4311/

Nomenclature

C_p	specific heat capacity of the battery, J kg^{-1} K^{-1}
E	emissivity
E_a	activation energy, kJ/mol
h	convective heat transfer coefficient, W m^{-2} K^{-1}
k_T	conductive heat transfer coefficient
L	thickness, m
R	universal gas constant, J mol^{-1} K^{-1}
T	surface temperature of battery, K
T_∞	free stream temperature, K
t	time, s
ρ	density of the battery, kg m^{-3}
r	radius of cell, m
σ	variance of the experimental results
σ_{sb}	Stefan–Boltzmann constant, W m^{-2} K^{-4}
$\overline{y}$	represents the average experimental results (y)

Subscript

eff	effective
i	different layer of active battery material
ang	angular direction
r	radial direction

or softening. These conditions are expected to be very challenging for the reliability of the polymer insulator. On the other hand, polymer insulator with poor thermal conductivity, together with high thermal contact resistance exist between the polymer insulator and battery metal casing that prevents the heat generated from the battery to dissipate effectively to the surroundings. The heat dissipation from the battery is realized by conduction across the actual contact area of the metal casing and polymer insulator and through conduction or radiation across the air gaps [4]. The contact area is normally small for rough surfaces. In addition, imperfect heat shrink process may introduce an air bubble being trapped between the battery metal casing and the insulator which leads to localized heat accumulation. During high I_t-rates of charging and discharging, the heat generated would be retained inside the cell. This is caused by thermal contact resistance between battery casing and polymer insulator, thus forming a large temperature gradient inside the cell under strong forced convection process [5]. Therefore, it is required to investigate these issues with insulator to ensure that the battery performs safely at all levels including electrical and thermal.

The properties of the metal surface could be changed by applying a layer of coating. The coating material properties could have an excellent thermal conductivity, good thermal insulating properties, electrically conductive or non-conductive [6]. Boron Nitride has a layer structure which is similar to graphite [7], and possesses a good thermal conductivity, electrical insulation, low dielectric constant and good thermal stability up to 1000 °C in the air [6]. Besides, Boron Nitride shows chemical inertness, high corrosion and erosion resistance. Due to these advantages, Boron Nitride has been used widely as release agents and protective coatings for dies/molds, glass making process, metal processing, sintering, welding, brazing, etc. Properties of Boron Nitride are shown in Table 1. There are various methods used for Boron Nitride coating such as chemical vapor deposition (CVD) [9–11], plasma assisted chemical vapor deposition (PACVD) [12–14], physical vapor deposition (PVD) [15–17], and spin coating [18]. However, studies on the Boron Nitride coating on the battery casing are rare. Moreover, most of the studies on the thermal analysis of Li-ion battery did not take the effect of the polymer insulator into account [19–23].

Taguchi technique is an experimental technique developed by Dr. Genichi Taguchi to dramatically improve the process, quality, product characteristics and simultaneously reduce the product development time and cost [24–26]. The principles of robust design are based on statistical methods to identify the parameters that affecting the performances. Besides, the optimum parameters determined from the laboratory level can be reproduced in the industrial conditions [27]. A full factorial design, which requires measuring all the design parameters, is costly and time consuming. However, by implementing Taguchi method, only a certain combination of parameters according to orthogonal array needs to be calculated and the target of the Taguchi method is to create a better parameter group and reduce the design period [25]. Hence, Taguchi method could be utilized to optimize the coating parameters effectively.

In the present study, the feasibility study to replace the polymer insulator of the battery with Boron Nitride coating will be investigated. A Taguchi method with orthogonal array L_9 (3^4) is used to optimize the coating parameters of the battery casing. Two factors, surface roughness of casing and coating thickness, which affect the coating quality are investigated. The target performance measure is used to determine the main control factors that largely affect the coating performance. The significance and contribution of each factor is analyzed using Analysis of Variance (ANOVA). Confirmation test is performed to validate the experimental design. Lastly, the influence of the conventional polymer insulator and Boron Nitride coating on the internal cell temperature distribution under various I_t-rates of constant current charging with forced convection will be discussed.

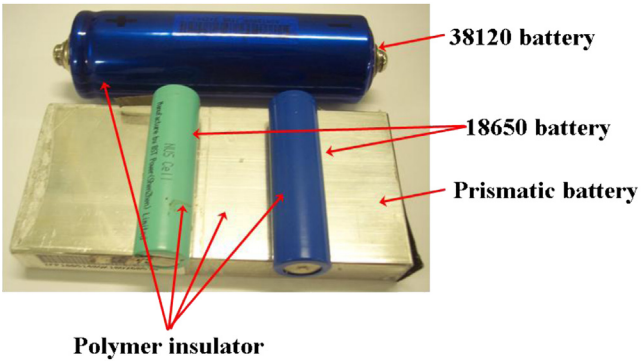

Fig. 1. Different types of Li-ion battery with polymer insulator.

Table 1
Properties of Boron Nitride [8].

Properties	Value
Crystal structure	Hexagonal
Color	White
Density, kg m^{-3}	1900
Maximum used temperature, °C	1800
Hardness, kg mm^{-2}	15–24
Elastic modulus, GPa	46.9
Thermal expansion coefficient (10^{-6}) (°C^{-1})	Parallel 11.9 Perpendicular 3.1
Thermal conductivity, W m^{-1} K^{-1}	Parallel 30 Perpendicular 33
Specific heat, J kg^{-1} K^{-1}	1610
Dielectric breakdown strength, ac-kV mm^{-1}	Parallel 95 Perpendicular 79
Vol resistivity, Ω cm	Parallel > 10^{14} Perpendicular > 10^{15}

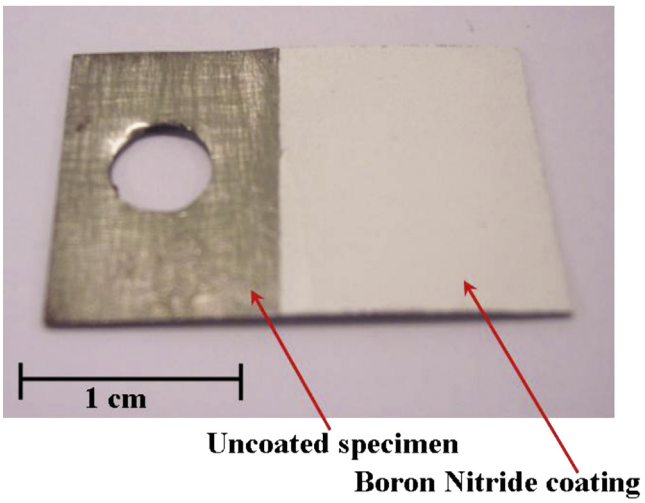

Fig. 2. Specimen.

2. Model development

2.1. Experimental setup and procedure

The most important assessment of coating performance is the adhesion strength. The coating studies were conducted using commercial 18650 Li-ion battery casings. The battery casings were flattened and cut to a size of 2 cm × 2 cm. The samples were polished with 300–1200 μm emery papers into different category of surface roughness. Next, samples were ultrasonically cleaned using water for 10 min followed by washing of the sample with ethanol. Mean absolute deviation of the sample surface roughness (R_a) was measured using a profilometer (Talysurf-120). Boron Nitride refractory paint (Alfa Aesar) is coated on the sample by spraying in the horizontal direction on the first layer and the vertical direction on the second layer to yield a uniform coating as shown in Fig. 2. The samples were dried in open air for 12 h. The thickness of the coating was measured using Scanning Electron Microscope (SEM) (JEOL JSM-5600 LV). Besides, the surface topology of the samples was also characterized by SEM and illustrated in Fig. 3. The left side of Fig. 3 shows the surface topology of the polished specimen. Scratch lines were formed on the surface by emery papers. On the other hand, the right side of Fig. 3 shows the surface topology of the specimen coated with Boron Nitride. No pores were formed on the coated specimen and the specimen was fully protected by Boron Nitride coating. Adhesion measurements were conducted using Nanoscratch tester (CSM Instruments). Besides, the current leakage test was carried out by subjecting the sample to an open circuit

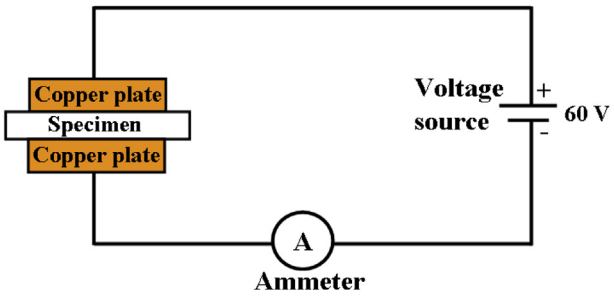

Fig. 4. Current leakage test.

voltage 0–60 V as shown in Fig. 4. The purpose of the current leakage test is to assess the quality of coating and ensure that no leakage current flow across the coated specimen. In addition, it is also used to determine the minimum coating thickness required for a given voltage before the insulation effect breakdown.

2.2. Design of experiment based on Taguchi method

Defining the quality characteristic is very important to the success of the experiment. The quality characteristic should be defined in term of quantifiable units. Besides, the quality characteristic is defined so that potential interactions between factors are minimized and additivity is assured [29]. Additionally, the parameters are selected in such a way that the influence of the noise factors on the variation of the system performance is reduced. In this study, the parameters to be examined are sample surface roughness and coating thickness. The parameters and the levels are tabulated in Table 2. To evaluate the effects of the parameters on performance characteristics (adhesion strength) and to optimize the parameters, orthogonal array L_9 (3^4) as shown in Table 3 is selected. L_9 (3^4) orthogonal array allows four 3-level factors to be considered in nine experiments. The design of experiment as follows: the first column was assigned to sample surface roughness (A), the second column was assigned to coating thickness (B) and the third column was assigned to (AB) to estimate the interaction between surface roughness and coating thickness. The experiments were performed for each combination of parameter and its level and repeated three times to obtain the average value of adhesion strength.

2.3. Analysis of the S/N ratio

There are two performance measures for Taguchi method analysis, which are noise performance measure (NPM) and target performance measure (TPM) [29]. NPM is a measure of the

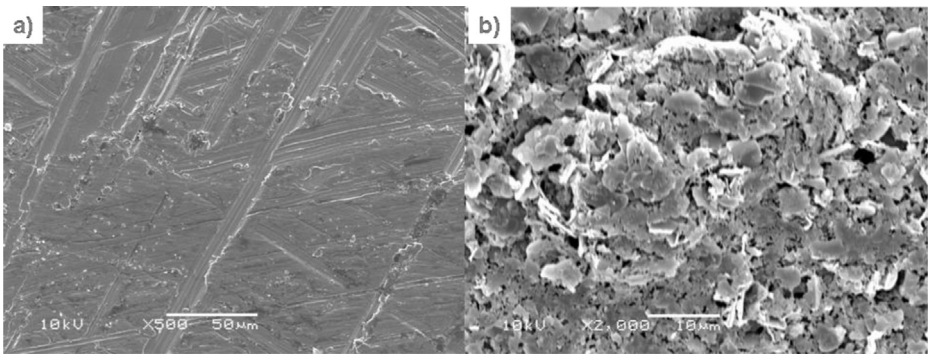

Fig. 3. (a) Typical SEM micrograph of uncoated specimen at magnification of 500×. (b) Typical SEM micrograph of coated specimen at magnification of 2000×.

Table 2
The parameters and their levels used in the experiments.

Parameters	Level		
	1	2	3
A: Surface roughness, μm	0.05–0.10	0.11–0.30	0.31–0.53
B: Coating thickness, mm	0.09–0.10	0.25–0.26	0.35–0.36

variation of the response and to identify the control factors that largely affect variation and it is termed as variability control factors [29]. The noise factors are external factors that will influence the outcome of the experimental results, but it is difficult to control in the field or the levels are expensive to control [29]. The TPM is a measure of the mean response and to identify the control factors that largely affect the mean and it is termed as target control factors [29]. In this study, the experimental observations are further transformed into a signal-to-noise (S/N) ratio. S/N ratio is the ratio of the mean (signal) to standard deviation (noise) and is used to evaluate the optimal parameters by taking the mean and variability into account [29]. There are three types of standard S/N ratios are generally used such as nominal the best, smaller the best and larger the best [29]. Since the coating thickness and surface roughness of the casing are proportional to the manufacturing cost and nominal the best is selected. Nominal the best as in Eq. (1) is chosen to obtain the optimum coating parameters [29].

Nominal the best:

$$\eta = 10\log_{10}\left(\frac{\bar{y}^2}{\sigma^2}\right) \tag{1}$$

$\bar{y}$ represents the average experimental results (y) of the adhesion strength under experimental conditions. While σ represents the variance of the experimental results y.

2.4. Analysis of variance

ANOVA is a key technique for analyzing the effect of categorical factors on a response [30]. ANOVA is used to analyze the results of the orthogonal array experiments by partitioning variability into identifiable sources of variation. Besides, the significant effect of the factor on the adhesion strength and the variation attributed by each factor can be rapidly identified, thus reduce the time required for experimental work [30]. The influential degree of each factor on the adhesion strength can be determined through the percentage of contribution of design parameters.

2.5. Thermal model

The thermal model of the 18,650 LFP cell is shown in Fig. 5. The battery consists of several layers of electrodes and separator wounded spirally into a cylinder. The cavity in the center of the cell is fully filled with electrolyte $LiPF_6$. In this study, the spiral wound region is assumed to be a single active material domain and the thermal conductivity is considered anisotropic because the thermal conductivity of the cell in the axial direction is higher than the radial direction [22]. The thermal conductivity of the cell in radial and axial direction is defined as in Eq. (2) [22]:

$$k_{T,r} = \frac{\sum L_i}{\sum L_i/k_{T,i}}, \quad k_{T,\mathrm{ang}} = \frac{\sum L_i k_{T,i}}{\sum L_i} \tag{2}$$

The thermal conductivity of the active material in the cell in x, y and z direction is defined as in Eq. (3) [22]:

$$\begin{aligned} k_{T,x} &= \frac{|y|}{r}\frac{\sum L_i k_{T,i}}{\sum L_i} + \frac{|x|}{r}\frac{\sum L_i}{\sum L_i/k_{T,i}}, \\ k_{T,y} &= \frac{|x|}{r}\frac{\sum L_i k_{T,i}}{\sum L_i} + \frac{|y|}{r}\frac{\sum L_i}{\sum L_i/k_{T,i}}, \quad k_{T,z} = \frac{\sum L_i k_{T,i}}{\sum L_i} \end{aligned} \tag{3}$$

The total density of the active material in the cell is expressed in equation below [22]:

$$\rho_{\mathrm{eff}} = \frac{\sum L_i \rho_i}{\sum L_i} \tag{4}$$

The total heat capacity of the active material in the cell is expressed in Eq. (5) below [22]:

$$C_{p,\mathrm{eff}} = \frac{\sum L_i C_{p,i}}{\sum L_i} \tag{5}$$

The physical and thermal properties of the 18,650 cell are presented in Table 6. The general energy equation used to model the heat conduction of the cell is defined in Eq. (6) [31].

$$\rho_{\mathrm{eff}} C_{p,\mathrm{eff}} \frac{\mathrm{d}T}{\mathrm{d}t} = \nabla \cdot k_{T,\mathrm{eff}} \nabla T + Q_{\mathrm{gen}} \tag{6}$$

With the boundary conditions at the outer surface of the cell is defined by Newton's cooling law and thermal radiation:

$$-k_{T,\mathrm{eff}} \left.\frac{\partial T}{\partial r}\right|_{r=R} = h(T - T_\infty) + E\sigma_{\mathrm{sb}}\left(T^4 - T_\infty^4\right) \tag{7}$$

Table 3
Orthogonal array for L_9 (3^4) for coating experiment and SNR values.

Experiment no.	A	B	A × B	$\bar{y}$, mN	S/N ratio (η)	Leakage, A
1	1	1	1	20.00	26.02	0
2	1	2	2	24.67	27.84	0
3	1	3	3	95.17	39.57	0
4	2	1	2	24.50	27.78	0
5	2	2	3	38.23	31.65	0
6	2	3	2	122.00	41.73	0
7	3	1	3	29.33	29.35	0
8	3	2	1	48.33	33.68	0
9	3	3	2	156.67	43.90	0

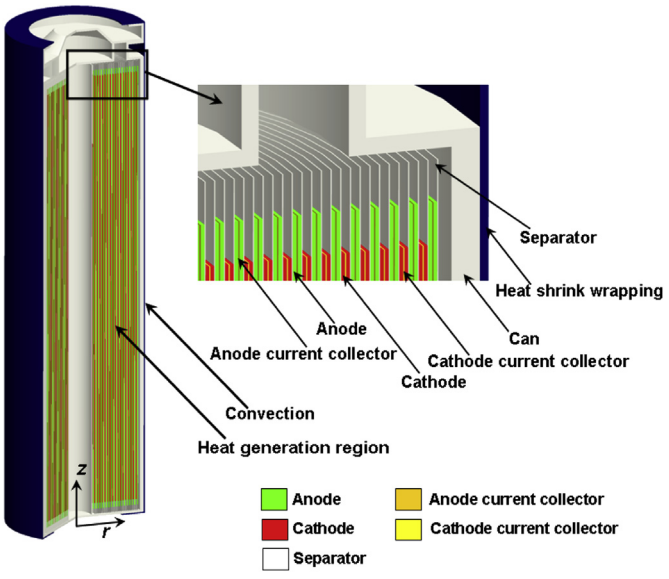

Fig. 5. Schematic of 18650 LFP cell thermal model.

Table 4
Average S/N ratios for adhesion strength.

Control factors	Average S/N ratios		
	A	B	AB
Level 1	27.51	25.32	30.37
Level 2	32.64	27.30	31.95
Level 3	31.34	38.88	29.17
Difference	4.50	13.56	2.78
Rank	2	1	
Characteristic type	Nominal the best		
Optimum	A2	B3	

Table 5
Results of the analysis of variance.

Source	Sum of squares, SS	Degree of freedom, d*f*	Variance, *V*	*F*-test	Contribution, %
A	4468.84	2	2234.42	34.41	7.21
B	53,454.01	2	26,727.00	411.56	88.61
AB	953.68	2	476.84	7.34	1.37
Error	1298.82	20	64.94	1.00	2.81
Total	60,175.34	26	2314.44	–	100.00
Mean	104,119.34	1	–	–	–
Total sum of squares	164,294.689	27	–	–	–

Heat generated of the cell during constant current charging at increasing state of charge is measured using accelerating rate calorimeter (ARC, THT). The charging of the single cell was carried out using 3 and 5 I_t-rates of constant current charging. The heat generated data were then input into the thermal model to predict the internal temperature of the cell. In the numerical modeling, the thermal resistance film gap for the imperfection of polymer insulator wrapping is assumed to be 0.3 mm based on a worst case scenario. The typical heat transfer coefficient for liquid cooling is within 100–20,000 W m^{-2} K^{-1} [4]. In the current study, a moderate liquid condition with $h = 500$ W m^{-2} K^{-1} is used in the modeling to compare the thermal performance of the cell using polymer insulator and Boron Nitride coating.

2.6. Numerical procedure

The thermal model of the 18650 cell, together with appropriate boundary conditions was solved with commercial finite element solver, COMSOL Multiphysics 4.3. Triangular element was used to mesh the geometry and direct solver PARDISO was chosen with a relative convergence tolerance of 10^{-6} for the modeling. All computations were carried out on a computer with a 3.40 GHz Quad core processor and 32 GB Random Access Memory (RAM). In addition, the grid independent test was carried out to refine the grid size of the model until the simulation results are not affected by further refinement of the mesh and error of the results is less than 5%.

3. Results and discussion

3.1. Analysis of the S/N ratio

The average S/N values obtained for each experiment are presented in Table 4 and Fig. 6. As shown in Fig. 6(a), the larger slope means that the effect of the control factor on the performance characteristic is more significant. Besides, the largest S/N ratio for each control factor provides an optimum performance. The effect of A is 5.13 dB while the effect of B is 13.56 dB. This also means that the coating thickness plays a more important role than surface roughness in affecting the adhesion strength. Increasing the thickness of coating to 0.35–0.36 mm will lead to increase in adhesion strength to 400% under experimental conditions. On the other hand, increasing the surface roughness of the sample of 0.53 μm will only lead to increase in adhesion strength to 68% under experimental conditions. Based on nominal the best transformation, the recommended optimal level of surface roughness of the sample is A2 (0.11–0.30 μm) and B3 (0.35–0.36 mm) for coating thickness. The interaction of factor A and B is illustrated in Fig. 6(b). Analysis of these interactions shows that there is a strong interaction on level 2 of factor A and B. Average S/N ratios for interaction AB on level 2 is 31.95 dB. On the other hand, the control factors have relatively weak interaction among each other on level 1 and level 3 but they do have an effect on the adhesion strength. As shown in Table 4, average S/N ratio of interaction AB at level 1 and level 3 is 30.37 dB and 29.17 dB respectively and lower than interaction AB at level 2.

3.2. Analysis of variance

The analysis of variance results of the analysis are presented in Table 5. *F*-test of 99% confidence is used as a reference tool to identify the significant factors that affect the performance characteristics in this study. An alpha-error of 1%, $\alpha = 0.01$, $v1 = 2$ and $v2 = 20$ is determined from the F-table and $F_{0.01,2,20} = 5.85$. Since factor A (34.41) and B (411.56) is much larger than 5.85, it can be inferred that factor A and B are significant. Moreover, interaction of A and B with *F*-ratio of 7.34 shows that interaction between A and B is significant and interdependent. Coating thickness was found to

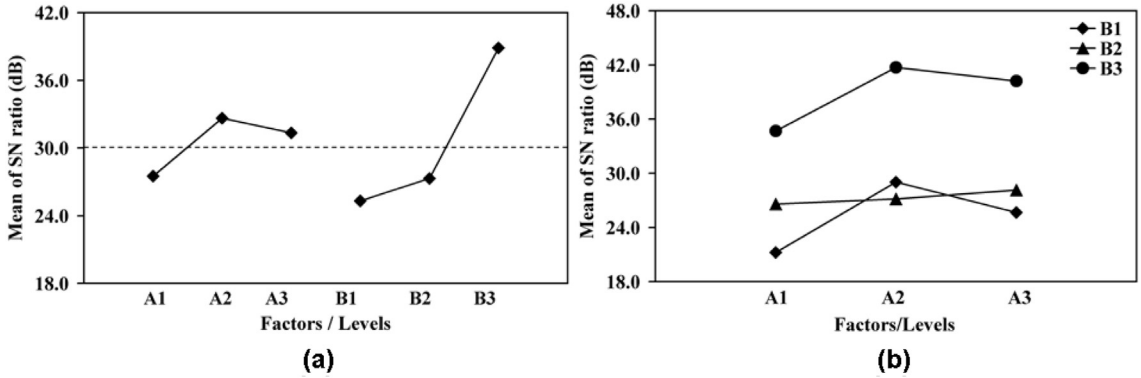

Fig. 6. (a) The effect of design parameters on adhesion strength. (b) Interaction graph of design parameter of A and B.

be the most significant parameter affecting the adhesion strength (88.61%). The contribution of surface roughness is about 7.21%. The contribution due to error provides an estimate of the sufficiency of the experiments. The error is referred to the unknown or uncontrolled factors. Hence, the contribution of the error can be employed as an effective tool to evaluate the sufficiency or insufficiency of the experiment. Since the contribution of error in this study is about 2.8%, which is low enough to indicate that the experiment is sufficient and no important factors have been overlooked (Table 5).

3.3. Confirmation tests

The optimum parameters are determined through the S/N ratio analysis and F-test in the ANOVA analysis. Next, the confirmation test is planned to predict and validate the improvements of the adhesion strength using the optimum parameters A2 and B3. This combination is found in the orthogonal array experiment (Trial number 9). The predicted mean of response (PV) can be calculated from the Eq. (8) [29]:

$$\mathrm{PV} = \overline{y} + (A2 - \overline{y}) + (B3 - \overline{y}) \tag{8}$$

The predicted mean of response is 124.09 mN. A confirmation run that generates the adhesion strength close to 124.09 mN would verify the assumptions of the Taguchi methods. Three experiments were carried out to verify the adhesion strength at optimum level of A2 and B3 and the value obtained were 123 mN, 125 mN and 129 mN with an average value of 125.67 mN. This suggests that the implementation of Taguchi method in optimizing the coating parameters is successful.

3.4. Thermal analysis of the battery

Fig. 7 shows the experimental results of the heat generated of the 18,650 cell during 3 and 5 I_t-rates of constant current charging. The maximum heat generated of the cell is 2.79 W and 4.89 W respectively for 3 and 5 I_t-rates of constant current charging. In addition, the effect of Boron Nitride coating on the temperature distribution across the 18650 Lithium Iron Phosphate cell under moderate liquid cooling condition with $h = 500\ \mathrm{W\ m^{-2}\ K^{-1}}$ were investigated. Fig. 8 shows the temperature distribution across the cell with conventional polymer insulator and battery casing coated

Table 6
Properties of Lithium Iron Phosphate cell [4,28,32,33].

Properties	Value
Active material density, kg m^{-3}	2680
Active material heat capacity, J kg^{-1} K^{-1}	950
Active material thermal conductivity (radial), W m^{-1} K^{-1}	0.2
Active material thermal conductivity (Axial), W m^{-1} K^{-1}	37.56
Casing material	Stainless steel
Casing density, kg m^{-3}	7900
Casing specific heat capacity, J kg^{-1} K^{-1}	515
Casing thermal conductivity, W m^{-1} K^{-1}	16.2
Insulator material	PVC
Insulator density, kg m^{-3}	1400
Insulator specific heat capacity, J kg^{-1} K^{-1}	900
Insulator thermal conductivity W m^{-1} K^{-1}	0.19
Electrolyte density, kg m^{-3}	1130
Electrolyte specific heat capacity, J kg^{-1} K^{-1}	2055
Electrolyte thermal conductivity W m^{-1} K^{-1}	0.6
Air thermal conductivity, W m^{-1} K^{-1}	0.026
Diameter of mandrel, m	0.0036
Diameter of active material, m	0.0171
Thickness of battery casing, m	0.00030
Thickness of insulator, m	0.00035

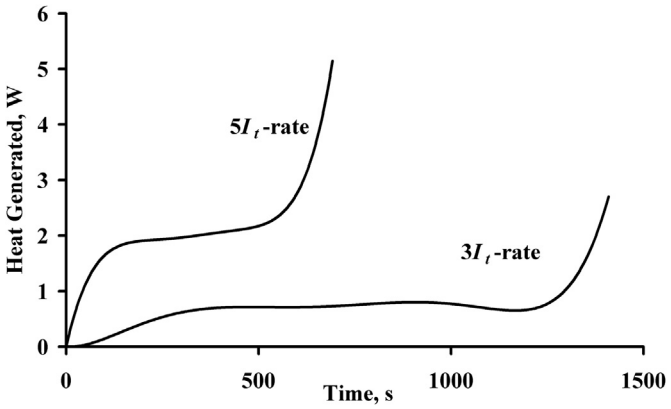

Fig. 7. Heat generated of the cell at 3 and 5 I_t-rates of charging.

with Boron Nitride at the end of the charging process. The maximum temperature is situated in the active material region near the center cavity. As shown in Fig. 8(a) and (b), the maximum temperature of the cell during 3 I_t-rates of constant current charging is effectively suppressed from 36.1 °C to 33.6 °C when the battery casing is coated with Boron Nitride. As shown in Fig. 8(c) and (d), for 5 I_t-rates of constant current charging, the temperature of the cell could reach 42.5 °C with conventional polymer insulator while the maximum temperature of the battery casing coated with Boron Nitride is only 36.9 °C. The optimum operating temperature of Li-ion battery is within 25 °C–40 °C for optimum performance and calendar life [34]. Hence, internal temperature of the cell casing coated with Boron Nitride is still within the optimum operating temperature of the Li-ion battery. Polymer insulator creates a thermal resistive film and prevents the heat generated from the cell being effectively dissipated to the outer environment and a large temperature gradient was developed inside the cell. According to Arrhenius law as in Eq. (9) [35], when the temperature of the cell is increased by 10–15 °C, the life cycle of the cell will decrease by about 30%–50%. For a prolonged period of operation, the internal resistance of the cell increases thus reducing the total charging capacity of the cell. Besides, the cell is more prone to thermal runway at high temperature [35].

$$k_{\mathrm{aging}} = \exp\left(-\frac{E_a}{RT}\right) \tag{9}$$

Hence, this is a significant adverse effect and should be accounted for the thermal management design of the Li-ion battery. The Boron Nitride coating will enhance the heat dissipation of the cell to the surroundings and also ensure good thermal contact between the battery and cold plate or cooling fin while maintaining adequate electric insulation.

A worth noting issue is the cost of the Boron Nitride coating, which may be higher than the polymer insulation. However, the cost increment according to the lab scale study is minimal (<5%) as compared to the cost of battery. The cost may be reduced during mass production stage. A cost effectiveness analysis may show that it is worthwhile to have Boron Nitride coating on batteries, especially fast charging battery.

4. Conclusion

In this study, the influence of the battery casing surface roughness and coating thickness of the Boron Nitride was optimized by the Taguchi experimental design method. The optimum parameters combination of casing surface roughness, coating

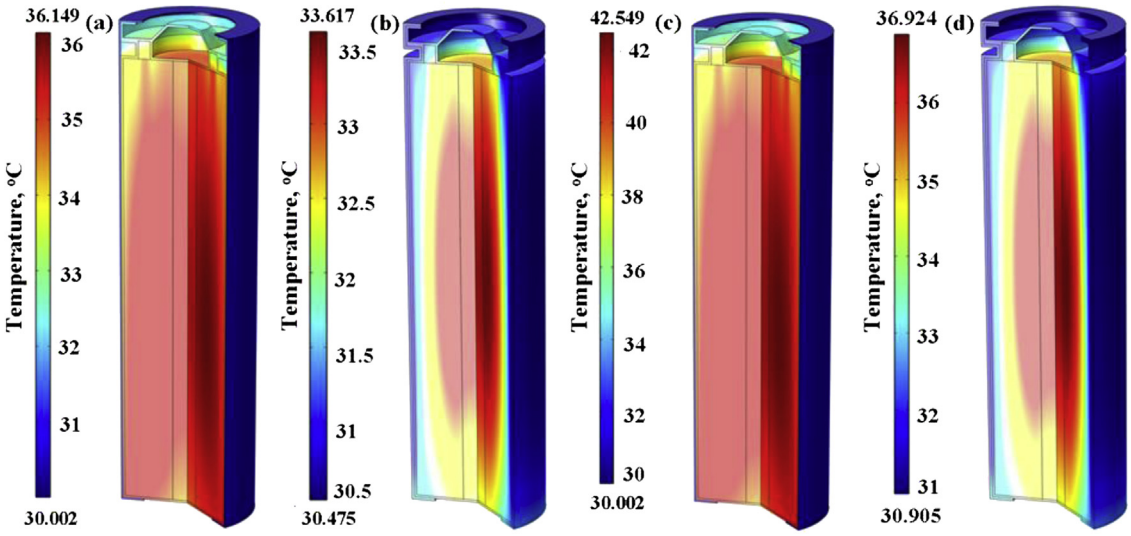

Fig. 8. Internal temperature distribution of the 18,650 cell. (a) 3 I_t-rate of constant current charging with polymer insulator. (b). 3 I_t-rate of constant current charging with Boron Nitride coating. (c) 5 I_t-rate of constant current charging with polymer insulator. (d). 5 I_t-rate of constant current charging with Boron Nitride coating.

thickness and the interaction of the parameters was obtained using analysis of S/N ratio and F-test. Nominal the best criteria were chosen to optimize the parameters to yield a minimum manufacturing cost and can be easily implemented in the industry. The significance of the factor and the contributions on the performance characteristic were determined from the ANOVA. All the parameters are considered to be confounded within 99% of confidence level. The most ideal candidate for optimum combination of parameters is A2 and B3 with surface roughness of 0.11–0.30 μm and coating thickness of 0.35–0.36 mm respectively. It is shown that the surface roughness of casing and coating thickness are correlated and they play a significant effect on the adhesion strength. At a high I_t-rate of charging process, the conventional polymer insulation may create a substantial temperature gradient inside the cell. This is not favored in the view of thermal management and cycle life of the cell. Moreover, the cell is more prone to thermal aging and thermal runway as compared to the battery casing coated with Boron Nitride. In addition, battery surface coated with Boron Nitride also enables the cold plate to be attached directly to the battery casing for effective heat dissipation.

Acknowledgements

This work was supported by a grant no. EPD090005RFP(A) from Energy Market Authority of Singapore.

References

[1] M.S. Wu, K.H. Liu, Y.Y. Wang, C.C. Wan, Heat dissipation design for lithium-ion batteries, J. Power Sources 109 (2002) 160–166.
[2] Q. Huang, M. Yan, Z. Jiang, Thermal study on single electrodes in lithium-ion battery, J. Power Sources 156 (2006) 541–546.
[3] R. Sabbah, R. Kizilel, J.R. Selman, S. Al-Hallaj, Active (air-cooled) vs. passive (phase change material) thermal management of high power lithium-ion packs: limitation of temperature rise and uniformity of temperature distribution, J. Power Sources 182 (2008) 630–638.
[4] F.P. Incropera, D.P. Dewitt, T.L. Bergman, A.S. Lavine, Fundamentals of Heat and Mass Transfer, sixth ed., John Wiley & Sons, Asia, 2007.
[5] J. Shi, F. Wu, S. Chen, C. Zhang, Thermal analysis of rapid charging nickel/metal hydride batteries, J. Power Sources 157 (2006) 592–599.
[6] S. Rudolph, Composition and application of coatings based on boron nitride, Interceram 42 (1993) 303–305.
[7] A. Lipp, K.A. Schwetz, K. Hunold, Hexagonal Boron nitride: fabrication, properties and application, J. Eur. Ceram. Soc. 5 (1989) 3–9.
[8] Accuratus, 2013. http://www.accuratus.com/boron.html (access August 2013).
[9] J.S. Li, C.R. Zhang, B. Li, F. Cao, S.Q. Wang, Boron nitride coatings by chemical vapor deposition from borazine, Surf. Coat. Technol. 205 (2011) 3736–3741.
[10] S.L. Gallet, G. Chollon, F. Rebillat, A. Guette, X. Bourrat, R. Naslain, M. Couzi, J.L. Bruneel, Microstructural and microtextural investigations of boron nitride deposited from BCl_3–NH_3–H_2 gas mixtures, J. Eur. Ceram. 24 (2004) 33–44.
[11] F. Ye, L. Zhang, Y. Liu, S. Li, M. Su, X. Yin, L. Cheng, Investigation on preparing boron nitride by nitriding pure boron at 1200–1550 °C, Prog. Nat. Sci. Mater. Int. 22 (2012) 433–439.
[12] I. Konyashin, J. Loeffler, J. Bill, F. Aldinger, A novel approach to deposition of cubic boron nitride coatings, Thin Solid Films 308–309 (1997) 101–106.
[13] I.H. Kim, K.S. Kim, S.H. Kim, S.R. Lee, Synthesis of cubic boron nitride films using a helicon wave plasma and reduction of compressive stress, Thin Solid Films 290–291 (1996) 120–125.
[14] D.R. McKenzie, W.D. McFall, S. Reisch, B.W. James, I.S. Falconer, R.W. Boswell, H. Persing, A.J. Perry, A. Durandet, Synthesis of cubic boron nitride thin films, Surf. Coat. Technol. 78 (1996) 255–262.
[15] M.A. Djouadi, A. Vasin, C. Nouveau, B. Angleraud, P.Y. Tessier, Deposition of boron nitride films by PVD methods: transition from h-BN to c-BN, Surf. Coat. Technol. 181–181 (2004) 174–177.
[16] I. Bello, Y.M. Chong, K.M. Leung, C.Y. Chan, K.L. Ma, W.J. Zhang, S.T. Lee, A. Layyous, Cubic boron nitride films for industrial applications, Diam. Relat. Mater. 14 (2005) 1784–1790.
[17] H. Jensen, G. Sorensen, Ion bombardment as a tool for duplex surface treatment in boron nitride film deposition, Surf. Coat. Technol. 84 (1996) 524–527.
[18] E. Husain, T.N. Narayanan, J.J.T. Tijerina, S. Vinod, R. Vajtai, P.M. Ajayan, Marine corrosion protective coatings of hexagonal boron nitride thin films on stainless steel, ACS Appl. Mater. Interfaces 5 (2013) 4129–4135.
[19] D.H. Jeon, S.M. Baek, Thermal modeling of cylindrical lithium ion battery during discharge cycle, Energy Convers. Manag. 52 (2011) 2973–2981.
[20] L. Cai, R.E. White, Mathematical modeling of a lithium ion battery with thermal effects in COMSOL Inc. Multiphysics (MP) software, J. Power Sources 196 (2011) 5985–5989.
[21] C. Forgez, D.V. Do, G. Friedrich, M. Morcrette, C. Delacourt, Thermal modeling of a cylindrical $LiFePO_4$/graphite lithium-ion battery, J. Power Sources 195 (2010) 2961–2968.
[22] S.C. Chen, Y.Y. Wang, C.C. Wan, Thermal analysis of spirally wound lithium batteries, J. Electrochem. Soc. 153 (2006) A637–A648.
[23] N. Sato, Thermal behavior analysis of lithium-ion batteries for electric and hybrid vehicles, J. Power Sources 99 (2001) 70–77 (2011).
[24] J.P. Ross, Taguchi Techniques for Quality Engineering, second ed., McGraw-Hill, New York, 1988.
[25] Q. Chen, M. Zeng, J. Zhang, Q. Wang, Optimal design of bi-layer interconnector for SOFC based on CFD-Taguchi method, Int. J. Hydrogen Energy 35 (2010) 4292–4300.
[26] E. Turgut, G. Cakmak, C. Yildiz, Optimization of concentric heat exchanger with injector turbulators by Taguchi method, Energy Convers. Manag. 53 (2012) 268–275.
[27] I. Kotcioglu, A. Cansiz, M.N. Khalaji, Experimental investigation for optimization of design parameters in a rectangular duct with plate-fins heat exchanger by Taguchi method, Appl. Therm. Eng. 50 (2013) 604–613.
[28] L.H. Saw, Y. Ye, A.O.O. Tay, Electrochemical-thermal analysis of 18,650 lithium iron phosphate cell, Energy Convers. Manag. 75 (2013) 165–172.
[29] N. Belavendram, Quality by Design, first ed., Prentice Hall, London, 1995.
[30] A. Bendell, J. Disney, W.A. Pridmore, Taguchi Methods: Applications in World Industry, first ed., Springer-Verlag, Berlin, 1989.

[31] W. Fang, O.J. Kwon, C.Y. Wang, Electrochemical thermal modeling of automotive Li-ion batteries and experimental validation using a three electrode cell, Int. J. Energy Res. 34 (2010) 107–115.
[32] M. Fleckenstein, O. Bohlen, M.A. Roscher, B. Baker, Current density and state of charge inhomogeneities in Li-ion battery cells with $LiFePO_4$ as cathode material due to temperature gradients, J. Power Sources 196 (2011) 4769–4778.
[33] S.C. Chen, C.C. Wan, Y.Y. Wang, Thermal analysis of lithium-ion batteries, J. Power Sources 140 (2005) 111–124.
[34] A.A. Pesaran, Battery thermal models for hybrid vehicle simulations, J. Power Sources 110 (2002) 377–382.
[35] Ch Kuper, M. Hoh, G.H. Miller, J. Fuhr, Thermal management of hybrid vehicle battery systems, in: Proc. EVS24, 2009.